

DOI [10.24425/ae.2021.137584](https://doi.org/10.24425/ae.2021.137584)

On magnetization deviations as the dominant cause for vibration harmonics in the spectrum of a PMSM drive

MARKUS JAEGER¹, PASCAL DRICHEL², MICHAEL SCHRÖDER¹, JOERG BERROTH²,
GEORG JACOBS², KAY HAMEYER¹

¹*Institute of Electrical Machines (IEM), RWTH Aachen University
Germany*

²*Institute of Systems Engineering and Machine Elements (MSE), RWTH Aachen University
Germany*

*e-mail: {markus.jaeger/michael.schroeder/Kay.Hameyer}@iem.rwth-aachen.de,
{pascal.drichel/joerg.berroth/georg.jacobs}@mse.rwth-aachen.de*

(Received: 08.02.2021, revised: 31.03.2021)

Abstract: Production deviations have a remarkable effect on the radiated sound of electrical machines, introducing additional signal components besides the fundamental field waves which significantly change and enrich the subjectively perceived sound characteristic. In literature these harmonics are mainly traced back to dynamic eccentricity, which modulates the fundamental field waves. In this paper a thorough mechanic and electromagnetic analysis of a modern, well-constructed traction drive (permanent magnet synchronous machine) is performed to show that for this typical rotor configuration dynamic eccentricity is negligible. Instead, deviations in the rotor magnetization are shown to be the dominant cause for vibration harmonics.

Key words: electric machines, electromagnetic fields, NVH, permanent magnet machines, permanent magnets, production deviations

1. Introduction

The sound spectrum of an electrical machine arises from the magnetic forces acting on rotors and stators, which themselves arise from the time and space dependent magnetic flux density waves in the airgap. For an ideal machine the orders of the travelling field waves can be calculated analytically, as performed for an induction machine in [1]. A good summary of the phenomena is



© 2021. The Author(s). This is an open-access article distributed under the terms of the Creative Commons Attribution-NonCommercial-NoDerivatives License (CC BY-NC-ND 4.0, <https://creativecommons.org/licenses/by-nc-nd/4.0/>), which permits use, distribution, and reproduction in any medium, provided that the Article is properly cited, the use is non-commercial, and no modifications or adaptations are made.

given by GIERAS in [2]. In the case of a permanent magnet synchronous machine (PMSM) with an integer-slot winding, only multiples of the pole pair number p are expected as harmonics of the magnetic rotor flux density distribution b at a given time t :

$$b(a, t) = \sum_k^{\infty} \hat{B}_k \cos(kpa + \omega t + \varphi_k), \quad k = 1, 2, 3, \dots \quad (1)$$

Herein B_k is the flux density amplitude and φ_k the offset of the k -th harmonic, α the rotation angle and ω the angular speed at that time. Due to the quadratic dependency between magnetic stress and magnetic flux density the observed force harmonics over time t at a given angle α (e.g. at a stator tooth) show twice the frequency of the field waves.

Fig. 1 shows the measured surface acceleration, which is a direct result from the exciting forces, for the analyzed PMSM with $p = 6$ pole pairs and $N = 36$ stator teeth. The harmonics with the highest amplitude can be seen to be the 12th, 24th, 36th etc., reaching 2 kHz, 4 kHz, 6 kHz etc. at a speed of 10 000 rpm, in accordance with the theory. However, a great number of harmonics with a smaller amplitude can be observed in between.

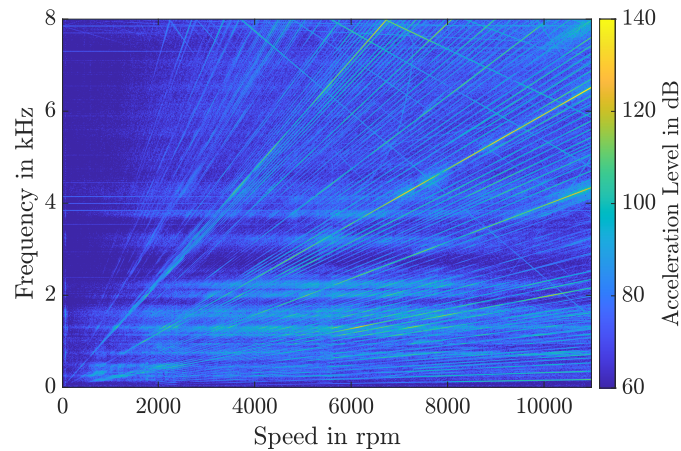


Fig. 1. Measured surface acceleration in radial direction on the housing of the analyzed PMSM

Some of these additional orders can arise from dynamic rotor eccentricity, as is shown in [2]. The eccentricity leads to additional field waves, modulating the fundamental wave. For the force, the additional orders as multiples of the rotation frequency are given by:

$$K = p \left(2k \pm \frac{1}{p} \right), \quad k = 1, 2, 3, \dots \quad (2)$$

In fact many publications can be found on the effects of static and dynamic eccentricity, e.g. in [3–5] or [6] and the detection of a faulty machine in [7, 8] or [9] due to the typical pattern of additional field harmonics that can be measured i. a. in the current or surface acceleration.

Deviations in the magnetization of the rotor of a PMSM, e.g. in remanence, in size or in the position of the magnets in the magnet pockets, cause comparable effects as rotor eccentricity by

altering the local magnetic flux density in the airgap. Accordingly, some publications can be found regarding magnetization or assembly faults, with a focus on fault detection in [10] or, e.g. the influence on the cogging torque in [11] (here in the case of 10% lower remanence in one magnet). However, the focus of most works is on explicit faults. Since magnet remanence and rotor assembly are subject to production deviations and statistical scattering, even in a machine referred to as “healthy”, magnetization deviations are present. A study of the influence of production deviations on cogging torque can be found in [12].

In this paper it is shown that a typical traction drive motor, which features a comparable rotor and bearing design as the studied one, exhibits a dynamic eccentricity close to zero. This is achieved by analyzing the rotor imbalance as well as the bearing clearance, and backed up by a very extensive modal analysis and elastic multi-body simulation (EMBS) of the complete drive train including a motor, gearbox, shaft system, housing and frame in operating conditions. Subsequently, a different explanation for the measured vibration harmonics is presented based on magnetization deviations of the rotor. Therefore, the relative magnetization deviations of the rotor poles are measured. Simulations of the tooth force done by finite element analysis (FEA) for different cases of high and low dynamic eccentricity with ideal magnets as well as with magnetization deviations according to the measurements are performed. A comparison to a measurement from search coils wound around stator teeth is presented to show that the magnetization deviation pattern matches the observed Fig. 1.

2. Determination of dynamic eccentricity

Dynamic eccentricity with regard to the airgap field of electrical machines describes any movement of the outer rotor contour (approximately a circle) which is no rotation around its center. There are three possible causes for dynamic eccentricity:

- static geometrical deformations: preexisting deviation between rotation axis and contour center,
- dynamic geometrical deformations: rotor vibrations,
- additional movement: movement of rotation axis.

While in principle this can be caused by a geometrical deformation (a shift of the outer rotor contour in one direction), the measurement of the rotor radius for the machine studied shows only localized deviations with a maximum of ± 0.06 mm with no general shift.

2.1. Rotor imbalance

Dynamic geometrical deformations and movement of the rotation axis require a causing force. While the magnetic forces can and do excite higher order rotor vibrations, due to the circular structure in the ideal case the resulting force cancels out leaving only shares from non-ideal behavior as excitation for bending of the rotor or movement of the rotation axis. Therefore, the main excitation mechanism is the centrifugal force from rotor imbalance.

Electrical machines with shaft height above 80 mm and speed above 950 rpm are typically balanced to the quality grade $G = 2.5$ mm/s in accordance with ISO 1940-1 [13], which incorporates most traction drives. The balance quality G is calculated from the speed ω , the imbalance

mass u referred to the rotor mass m and the radius r at which the imbalance mass rotates:

$$G = \frac{u}{m} \times r \times \omega. \quad (3)$$

The centrifugal F_{imb} is equivalent to the product of the rotating mass u , radius r and square of the angular speed ω^2 .

$$F_{\text{imb}} = u \times r \times \omega^2. \quad (4)$$

With Eq. (3) and Eq. (4) the dependency of the centrifugal force to the balance grade can be deduced:

$$F_{\text{imb}} \frac{G \times m}{\omega} \times \omega^2 = G \times m \times \omega. \quad (5)$$

The comparison in Fig. 2(a) between the centrifugal force and the gravitational force holding the rotor in place shows, that up to a speed of about 37 000 rpm the pull from the imbalance alone is not strong enough to lift the rotor.

Measurement of the rotor imbalance shows, that it indeed achieves balance quality grade 2.5 mm/s, as can be seen in Fig. 2(b).

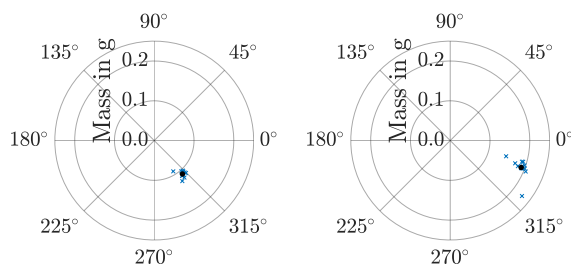
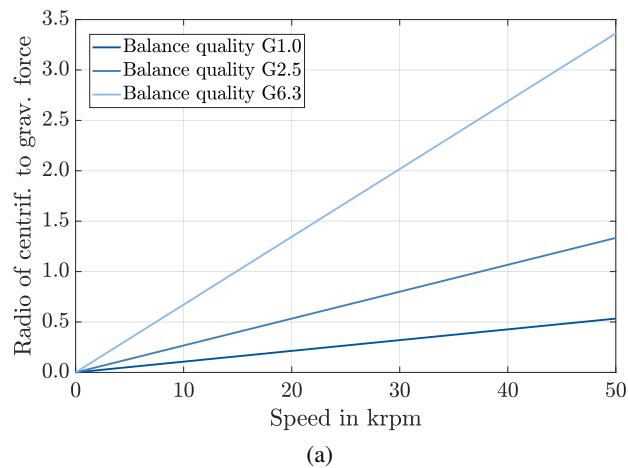


Fig. 2. (a) Ratio of centrifugal to gravitational force for different balance quality grades; (b) Multiple measurements (blue) of rotor imbalance at the two bearing planes for a mass at 50 mm radius, mean value of measurements in black

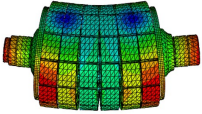
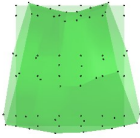
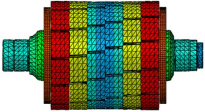
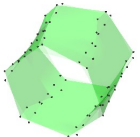
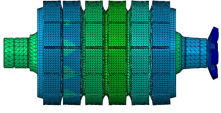
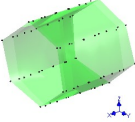
2.2. Bearing

In reality, dynamic eccentricity can occur at speeds significantly lower than 37 000 rpm due to vibrations of the rotor and friction in the bearings. The friction causes the rotor to ‘crawl’ up in the bearing and fall back, until the frictional forces, which rise with the speed, are high enough to result in full dynamic eccentricity. However, this requires the existence of bearing clearance to give room for movements. Bearing clearance is present in standard ball bearings due to manufacturing tolerances. It can, e.g. be removed by using an appropriate bearing arrangement (O or X-arrangement) and preloading it with so-called *bearing preload wave springs*. These springs are commonly available [14] and were used in the studied motor with X-arrangement, leading to a preloaded bearing arrangement, leaving no bearing clearance for dynamic eccentricity.

2.3. Elastic multi-body simulation

To substantiate the hypothesis of negligible dynamic eccentricity, a modal analysis of every part of the drive train was performed to establish a comprehensive EMBS. This allows to predict the dynamic movement of the rotor under operational conditions. Exemplarily, in Table 1. some measured modes of the rotor are shown in comparison to the FEA model which was reduced to be used in the EMBS.

Table 1. Comparison of rotor model to measurements

Simulation	Measurement	Rel. error
 3753 Hz	 3741 Hz	0.32%
 3919 Hz	 4022 Hz	-2.56%
 5601 Hz	 5500 Hz	1.84%

To illustrate the simulated drive train, Fig. 3(a) shows its assembly with the electric machine, the two-stage gearbox (gears colored in green and red), the semi-transparent housing group which

holds the bearings (blue) for all rotating parts which is itself mounted in the frame (black). The orange power cables and some red acceleration sensors are also visible.

For the application of the magnetic forces and the modeling of eccentricity, torsion and bending the rotor is modeled with the multi-slice method, discretizing it in the axial direction in six slices analogous to the real rotor assembly which is also constructed from six slices.

Throughout this paper, the eccentricity radius is given as percentage of the airgap length, meaning that 100% eccentricity equals a rotor slice displacement of 0.7 mm for the regarded machine, resulting in contact between the rotor and stator. In Fig. 3(b) the center position of the six slices is plotted in cylindrical coordinates for the startup to 4500 rpm under rated load. It can be seen that, besides the static eccentricity of about 8%, the slice radius (left axis) does vary less than 1% over time while the slice angle (right axis) varies about 1° . This shows that very little general rotor movement is happening in the simulation, including rotor vibrations and eccentricity. This backs up the analytical estimations, which predicted a dynamic eccentricity close to zero.

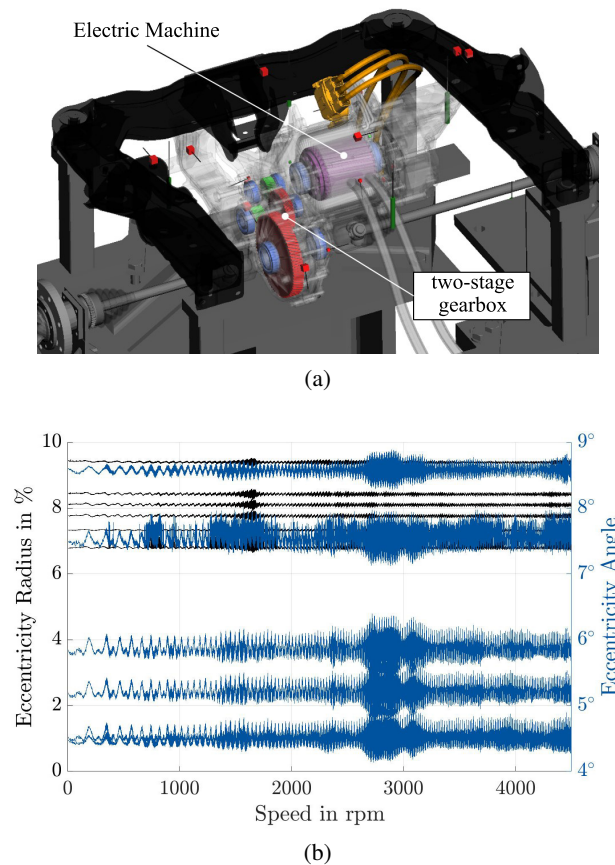


Fig. 3. (a) EMBS model of drive train; (b) Eccentricity of the six rotor slices over the course of the simulated run-up in cylindrical coordinates with radius in left axis and angle on right axis

3. Determination of magnetization deviations

The relative magnetization of the rotor poles was measured using a setup with a search coil without a magnetic core while spinning the rotor. This allows one to measure the flux linkage relativity between the rotor poles. The absolute flux cannot be measured with this setup.

Assuming the permanent magnet remanence is directly proportional to the measured flux linkage, and further assuming a normal distribution, this normal distribution around the nominal data sheet remanence value can be calculated as shown in Fig. 4. The first assumption neglects the effects of geometrical deviations of the rotor iron, permanent magnet position or more complex magnetization deviations (e.g. the direction). In this analysis all these effects influence the calculated distribution of the permanent magnet remanence, widening the distribution to some extent. To examine the contributions of the different deviations further work is necessary.

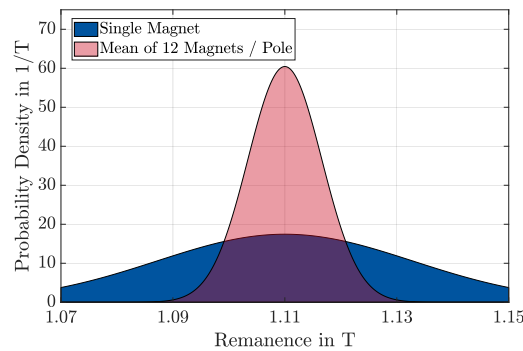


Fig. 4. Probability density calculated from measurements of the twelve rotor poles, and concluded probability density of individual permanent magnets, of which twelve single magnets create a pole

The normal distribution of the single magnet remanence can be calculated from the distribution of the pole's remanence, by using the number of permanent magnets which form one rotor pole. The result in Fig. 4 is in good accordance with the manufacturer data sheet, showing the nominal minimal and maximal values at about 2.5σ .

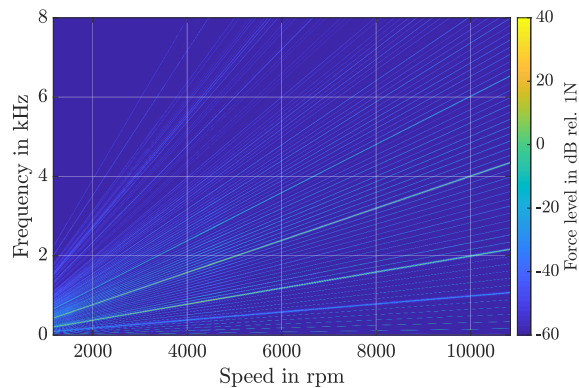
4. Measurement of tooth force

Three search coils around stator teeth were installed in the studied machine, each coil 9 teeth apart, i.e. 90° mechanical for the stator with 36 teeth. For the no load case, a primarily radial flux direction can be assumed. This allows one to connect the measured voltage, and, by integration of it, the measured flux, to the flux density and further to the radial tooth force.

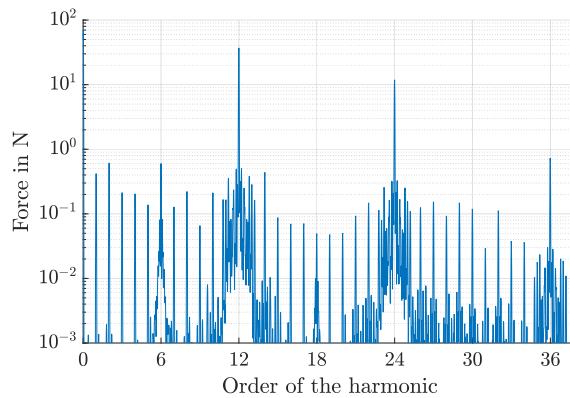
The search coil integrates the flux over the length of the machine, which is a function of the axial length due to the continuously skewed stator. The spectrogram of the measured tooth force over a no-load startup is shown in Fig. 5(a). As expected, the main harmonics are in accordance with the theory and the measurement of the surface acceleration in Fig. 1. However, the surface

acceleration is a superposition of all tooth forces at the 36 stator teeth in interaction with the structure dynamics response, which leads to the higher amplitude of the 36th and higher orders.

Since in the spectrogram in Fig. 5(a) no significant dependency of the speed is visible, an optically more precise comparison of the force harmonics at a fixed speed is shown in Fig. 5(b).



(a)



(b)

Fig. 5. (a) Mean radial tooth force from measurement of induced voltage using a search coil, run-up in no load case; (b) Spectrum of the mean radial tooth force from measurement of induced voltage referenced to rotational frequency, therefore the 12th harmonic (due to six pole pairs) is the base force frequency

5. Simulation

In the measured tooth force, harmonics besides the fundamental waves are visible. In addition to the finding, that magnetization deviations are present while dynamic eccentricity is not, the average tooth force is simulated for a qualitative comparison of the harmonic pattern to the measurement from the search coils. Therefore, a 2D finite element analysis for different cases of eccentricity and magnetization deviations is performed. The nodal forces were calculated by using

the eggshell method [15] and summed up to tooth forces using the method from [16], as shown in Fig. 6(a). The skew was introduced by averaging the 2D discrete forces over 60 appropriately rotated slices.

Fig. 6(b) shows the simulated spectrum of radial tooth force in the unrealistic case of 30% dynamic eccentricity with ideal magnets, to demonstrate its effect. Many additional harmonics with high amplitude are visible, with the highest harmonic amplitudes next to the fundamental orders.

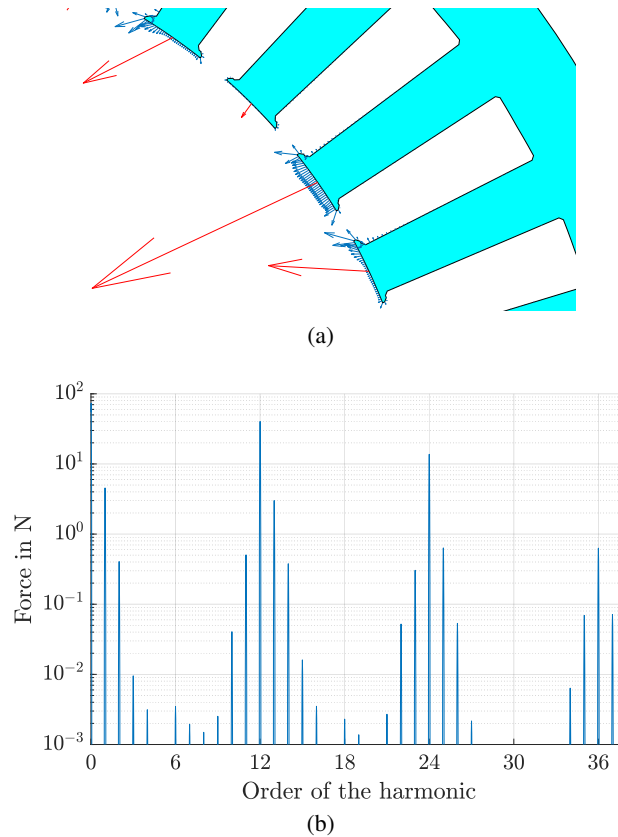


Fig. 6. (a) Nodal forces from FEA (blue vectors) and resulting tooth forces (red vectors) at no rotational position; (b) Spectrum of the radial tooth force for 30% dynamic eccentricity

Since the machine analysis in section 2.1 resulted in a dynamic eccentricity close to zero, a simulation for 3% dynamic eccentricity is shown in Fig. 7(a). As can be seen, the amplitude of most harmonics dropped below the 0.01 N mark, with only some left with frequencies next to the fundamental orders. While the spectrogram with 30% eccentricity in Fig. 6(b) shows a lot of harmonics which could possibly explain the measured surface acceleration (compare Fig. 1), the expected eccentricity of 3% or less cannot. Further, the pattern of the spectrum from 30% eccentricity does not match well to the measured force spectrum in Fig. 5.

Finally, a simulation without dynamic eccentricity but with magnetization deviations is shown in Fig. 7(b). The remanence of the single permanent magnets is randomly chosen from the normal distribution in Fig. 4. The spectrogram shows a wide range of harmonics. In contrast to the dynamic eccentricity cases the orders with the highest amplitudes are not necessarily close to the fundamental orders. The observed pattern of the harmonics does show good accordance with the measurement from the search coil in Fig. 5(b), but many harmonics have a lower amplitude than in the measurement. Despite the deviations in magnet remanence, the simulation is too ideal due to neglecting any other production deviations.

For comparability a spectrogram of the simulation with magnetization deviations is also given in Fig. 7(c). The higher orders visible in the measured spectrogram are caused by small deviations in the magnet's position or rotor iron geometry, which are not covered by the simulation, wherefore they are not visible here.

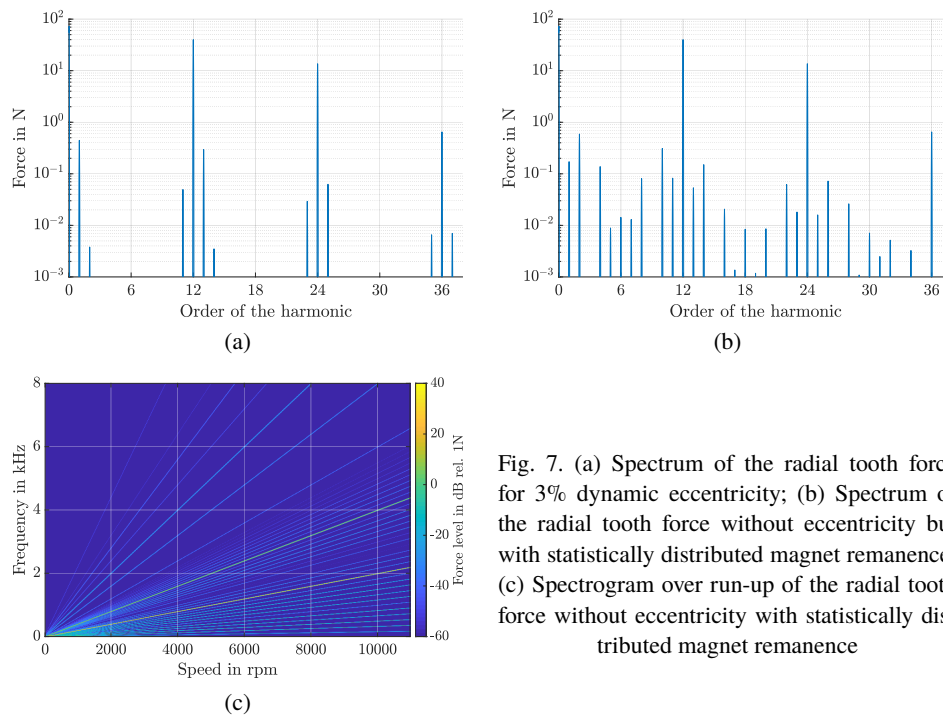


Fig. 7. (a) Spectrum of the radial tooth force for 3% dynamic eccentricity; (b) Spectrum of the radial tooth force without eccentricity but with statistically distributed magnet remanence; (c) Spectrogram over run-up of the radial tooth force without eccentricity with statistically distributed magnet remanence

In Fig. 8 additionally the waveform of the measured tooth force from the three search coils is plotted as well as the simulated tooth force for 30% dynamic eccentricity and the simulation with magnetization deviations. The simulation, in general, slightly overestimates the force, which can be caused, e.g. by the modelled magnetization curve for the soft magnetic material being higher than in reality.

By precisely measuring the remanence of each individual permanent magnet in the rotor as well as magnetization curve, and modelling each permanent magnet position inside its pocket, the measured tooth force could be reproduced with very little error for this exact machine.

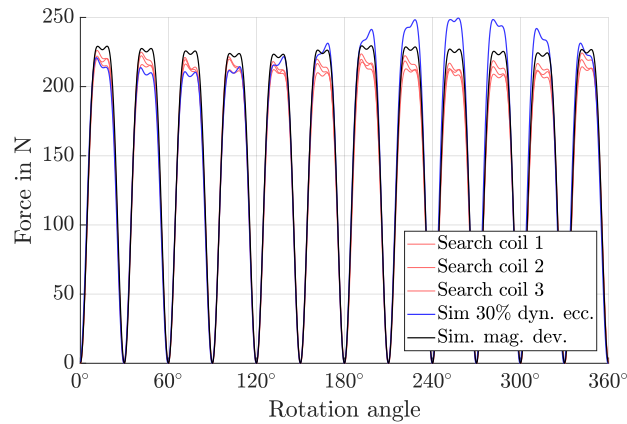


Fig. 8. Waveform of the radial tooth force over one full rotation at no load

6. Conclusion

In this paper it is shown that the vibration harmonics which can be measured on the surface of a typical PMSM drive are caused by rotor magnetization deviations instead of eccentricity. It is demonstrated that the rotor does not exhibit dynamic eccentricity. To generalize this

- a rotor construction of punched sheet metal, buried magnets and turned shaft,
- balancing according to standards,
- and a classic fixed/free preloaded bearing arrangement

is assumed and analyzed. The magnetization deviations of the rotor poles are measured. By assuming a normal distribution, the calculated single permanent magnet remanence distribution shows good accordance with the manufacturer data. FEA simulations of the tooth forces for cases of high and low dynamic eccentricity as well as magnetization deviations are compared to measurements of search coils wound around a tooth, which additionally support the hypothesis that indeed magnetization deviations and not dynamic eccentricity causes force and vibration harmonics.

Acknowledgements

This research was supported by the program for *Cooperative Industrial Research* (IGF funding no. 18764 N) with funding from the *German Federal Ministry for Economic Affairs and Energy* (BMWi) on the basis of a decision by the German Parliament. The authors further thank the *German Research Association* (Deutsche Forschungsgemeinschaft, DFG) for the support of the interdisciplinary research in the post graduate program *mobilEM* (GRK 1856).

Additionally, the authors further want to thank the *Forschungsvereinigung Antriebstechnik e.V.* (FVA) for the realization of the research project FVA 682 II and the support from experts of the FVA network.

Supported by:



Federal Ministry
for Economic Affairs
and Energy

on the basis of a decision
by the German Bundestag

References

- [1] Nahlaoui M.A., Steins H., Kulig S., Exnowski S., *Comparison of numerically determined noise of a 290 kW induction motor using FEM and measured acoustic radiation*, Archives of Electrical Engineering, vol. 62, pp. 195–207 (2013), DOI: [10.2478/ae-2013-0015](https://doi.org/10.2478/ae-2013-0015).
- [2] Gieras J.F., Wang C., Cho Lai J., *Noise of polyphase electric motors*, CRC Press Taylor and Francis Group (2006).
- [3] Hu Y., Wei H., Chen H., Sun W., Zhao S., Li L., *Vibration Study of Permanent Magnet Synchronous Motor Base on Static Eccentricity Model*, 22nd International Conference on Electrical Machines and Systems (ICEMS), Harbin, China, pp. 1–5 (2019), DOI: [10.1109/ICEMS.2019.8922162](https://doi.org/10.1109/ICEMS.2019.8922162).
- [4] Li Y., Wu H., Xu X., Cai Y., Sun X., *Analysis on electromechanical coupling vibration characteristics of in-wheel motor in electric vehicles considering air gap eccentricity*, Archives of Electrical Engineering, vol. 5, pp. 851–862 (2019), DOI: [10.24425/bpasts.2019.130882](https://doi.org/10.24425/bpasts.2019.130882).
- [5] Lundin U., Wolfbrandt A., *Method for Modeling Time-Dependent Nonuniform Rotor/Stator Configurations in Electrical Machines*, IEEE Transactions on Magnetics, vol. 45, iss. 7, pp. 2976–2980 (2009), DOI: [10.1109/TMAG.2009.2015052](https://doi.org/10.1109/TMAG.2009.2015052).
- [6] Zhang M., Macdonald A., Tseng K.-J., Burt G.M., *Magnetic Equivalent Circuit Modeling for Interior Permanent Magnet Synchronous Machine under Eccentricity Fault*, 48th International Universities' Power Engineering Conference (UPEC), Dublin, Ireland, pp. 1–6 (2013), DOI: [10.1109/UPEC.2013.6715044](https://doi.org/10.1109/UPEC.2013.6715044).
- [7] Ebrahimi B.M., Faiz J., Roshtkhari M.J., *Static-, Dynamic-, and Mixed- Eccentricity Fault Diagnoses in Permanent-Magnet Synchronous Motors*, IEEE Transactions on industrial electronics, vol. 56, no. 11, pp. 4727–4739 (2009), DOI: [10.1109/TIE.2009.2029577](https://doi.org/10.1109/TIE.2009.2029577).
- [8] Rosero J.A., Cusido J., Garcia A., Ortega J.A., Romeral L., *Broken Bearings and Eccentricity Fault Detection for a Permanent Magnet Synchronous Motor*, 32nd Annual Conference on IEEE Industrial Electronics (IECON), Paris, France, pp. 964–969 (2006), DOI: [10.1109/IECON.2006.347599](https://doi.org/10.1109/IECON.2006.347599).
- [9] Ilamparithi T., Nandi S., *Saturation independent detection of dynamic eccentricity fault in salient-pole synchronous machines*, IEEE International Symposium on Diagnostics for Electric Machines, Power Electronics and Drives (SDEMPED), Valencia, Spain, pp. 336–341 (2013), DOI: [10.1109/DEMPED.2013.6645737](https://doi.org/10.1109/DEMPED.2013.6645737).
- [10] Goktas T., Zafarani M., Akin B., *Discernment of Broken Magnet and Static Eccentricity Faults in Permanent Magnet Synchronous Motors*, IEEE Transactions on Energy Conversion, vol. 31, iss. 2, pp. 578–587 (2016).
- [11] Coenen I., van der Giet M., Hameyer K., *Manufacturing Tolerances: Estimation and Prediction of Cogging Torque Influenced by Magnetization Faults*, IEEE Transactions on Magnetics, vol. 48, iss. 5, pp. 1932–1936 (2012), DOI: [10.1109/TMAG.2011.2178252](https://doi.org/10.1109/TMAG.2011.2178252).
- [12] Gasparin L., Fiser R., *Cogging torque sensitivity to permanent magnet tolerance combinations*, Archives of Electrical Engineering, vol. 62, pp. 449–461 (2013), DOI: [10.2478/ae-2013-0036](https://doi.org/10.2478/ae-2013-0036).
- [13] International Organization for Standardization, *ISO 1940-1: Mechanical vibration — Balance quality requirements for rotors in a constant (rigid) state*, Geneva, Switzerland (2003).
- [14] <https://www.smalley.com/wave-springs/bearing-preload>, accessed March 2020.
- [15] Henrotte F., Felden M., van der Giet M., Hameyer K., *Electromagnetic force computation with the Eggshell method*, 14th International Symposium on Numerical Field Calculation in Electrical Engineering (IGTE), Graz, Austria (2010).
- [16] Herold T., Franck D., Schröder M., Böhmer S., Hameyer K., *Transientes Simulationsmodell für die akustische Bewertung elektrischer Antriebe*, e & i Elektrotechnik und Informationstechnik, vol. 133, no. 2, pp. 55–64 (2016).